JACS
JOURNAL OF THE AMERICAN CHEMICAL SOCIETY

ARTICLE

pubs.acs.org/JACS

Equilibration of Tyrosyl Radicals ($Y_{356}^{\bullet}$, $Y_{731}^{\bullet}$, $Y_{730}^{\bullet}$) in the Radical Propagation Pathway of the *Escherichia coli* Class Ia Ribonucleotide Reductase

Kenichi Yokoyama,[†] Albert A. Smith,[†,§] Björn Corzilius,[†,§] Robert G. Griffin,[†,§] and JoAnne Stubbe*[,†,‡]

[†]Department of Chemistry, [‡]Department of Biology, and [§]Francis Bitter Magnet Laboratory, Massachusetts Institute of Technology, 77 Massachusetts Avenue, Cambridge, Massachusetts 02139-4307, United States

Supporting Information

ABSTRACT: *Escherichia coli* ribonucleotide reductase is an $\alpha2\beta2$ complex that catalyzes the conversion of nucleotides to deoxynucleotides using a diferric tyrosyl radical ($Y_{122}^{\bullet}$) cofactor in $\beta2$ to initiate catalysis in $\alpha2$. Each turnover requires reversible long-range proton-coupled electron transfer (PCET) over 35 Å between the two subunits by a specific pathway ($Y_{122}^{\bullet} \leftrightarrows [W_{48}?] \leftrightarrows Y_{356}$ within β to $Y_{731} \leftrightarrows Y_{730} \leftrightarrows C_{439}$ within α). Previously, we reported that a $\beta2$ mutant with 3-nitrotyrosyl radical ($NO_2Y^{\bullet}$; 1.2 radicals/$\beta2$) in place of $Y_{122}^{\bullet}$ in the presence of $\alpha2$, CDP, and ATP catalyzes formation of 0.6 equiv of dCDP and accumulates 0.6 equiv of a new $Y^{\bullet}$ proposed to be located on Y_{356} in $\beta2$. We now report three independent methods that establish that Y_{356} is the predominant location (85−90%) of the radical, with the remaining 10−15% delocalized onto Y_{731} and Y_{730} in $\alpha2$. Pulsed electron−electron double-resonance spectroscopy on samples prepared by rapid freeze quench (RFQ) methods identified three distances: 30 ± 0.4 Å (88% ± 3%) and 33 ± 0.4 and 38 ± 0.5 Å (12% ± 3%) indicative of $NO_2Y_{122}^{\bullet}-Y_{356}^{\bullet}$, $NO_2Y_{122}^{\bullet}-NO_2Y_{122}^{\bullet}$, and $NO_2Y_{122}^{\bullet}-Y_{731(730)}^{\bullet}$, respectively. Radical distribution in $\alpha2$ was supported by RFQ electron paramagnetic resonance (EPR) studies using Y_{731}(3,5-F_2Y) or Y_{730}(3,5-F_2Y)-$\alpha2$, which revealed $F_2Y^{\bullet}$, studies using globally incorporated [β-$^2H_2$]Y-$\alpha2$, and analysis using parameters obtained from 140 GHz EPR spectroscopy. The amount of $Y^{\bullet}$ delocalized in $\alpha2$ from these two studies varied from 6% to 15%. The studies together give the first insight into the relative redox potentials of the three transient $Y^{\bullet}$ radicals in the PCET pathway and their conformations.

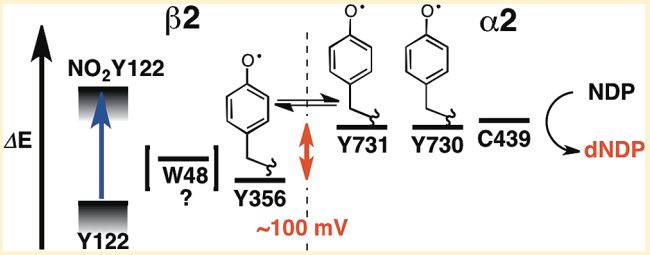

INTRODUCTION

Class Ia ribonucleotide reductases (RNRs) catalyze the reduction of nucleoside 5′-diphosphates (NDPs) to 2′-deoxynucleoside 5′-diphosphates (dNDPs) in all organisms and thereby provide the monomeric building blocks required for DNA replication and repair and control their relative ratios, essential for the fidelity of these processes.[1,2] *Escherichia coli* RNR consists of two homodimeric subunits, $\alpha2$ and $\beta2$. $\alpha2$ houses the binding sites for substrates (S's; UDP, CDP, ADP, or GDP) and effectors (E's; ATP, dATP, TTP, or dGTP) that control the specificity and rate of nucleotide reduction. $\beta2$ harbors the diferric tyrosyl radical ($Y_{122}^{\bullet}$) cofactor, which reversibly and transiently oxidizes C_{439} in the active site of $\alpha2$, which then initiates nucleotide reduction. A docking model of the active $\alpha2\beta2$ complex was first proposed by Uhlin and Eklund[3] using the shape complementarity of the individual crystal structures of each subunit, in which Y_{122} in $\beta2$ is >35 Å from C_{439} in $\alpha2$. This distance is too large for the oxidation to occur by electron tunneling, given the enzyme's turnover number of 2−10 s^{-1}, and thus, these observations led to the proposal[3,4] that the radical propagation proceeds by a hopping mechanism through conserved aromatic amino acid residues located in $\alpha2$ and $\beta2$ (Figure 1). Our recent studies[5] showed that a new $Y^{\bullet}$ is formed when a mutant $\beta2$ with a 3-nitrotyrosyl radical ($NO_2Y^{\bullet}$) in place of $Y_{122}^{\bullet}$ ([$NO_2Y_{122}^{\bullet}$]-$\beta2$) is incubated with $\alpha2$, CDP, and ATP. In this paper we report the use of three independent methods, pulsed electron−electron double resonance (PELDOR) spectroscopy, site-specific incorporation of 3,5-F_2Y (F_2Y) in place of Y_{731}- or Y_{730}-$\alpha2$, and global incorporation of [β-$^2H_2$]Y-$\alpha2$, to establish that the newly trapped $Y^{\bullet}$ is predominantly located at Y_{356} in $\beta2$ (~87%) and is also delocalized into Y_{731} and Y_{730} in $\alpha2$ (~13%).

Figure 1 shows our current proposal[6] for the radical propagation steps in RNR where the oxidation of C_{439} by $Y_{122}^{\bullet}$ occurs in multiple steps involving orthogonal or colinear proton-coupled electron transfer (PCET) (Figure 1). Mechanistic studies of this process were initially hampered by the rate-limiting protein conformational change(s) (2−10 s^{-1}) triggered by substrate and effector binding to $\alpha2$ that precedes the radical propagation process and consequently masks all the subsequent steps.[7] While initial mutagenesis studies suggested the importance of the residues in the pathway,[8,9] the mutant's inactivity precluded mechanistic studies. Thus, to investigate the mechanism, our laboratory has utilized Y analogues with different redox

Received: August 17, 2011
Published: October 03, 2011

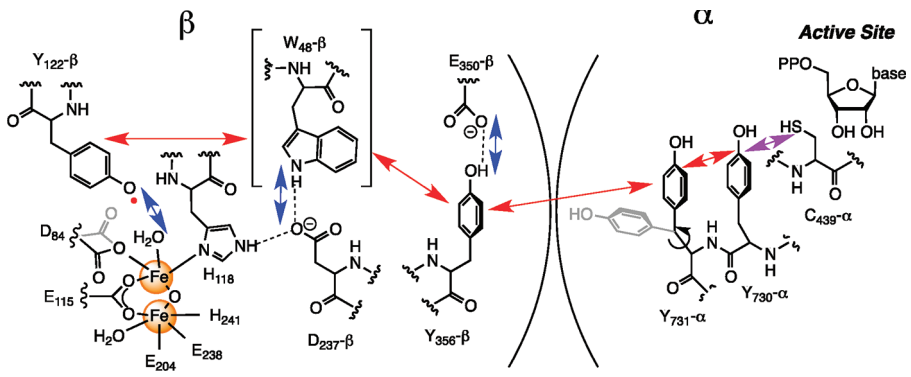

Figure 1. Proposed PCET pathway in *E. coli* class Ia RNR. Alternative conformations found in crystal structures are shown in gray for D_{84}-β2 (PDB ID 1JQC[61]) and Y_{731}-α2 (PDB ID 2XO4[42]). Red and blue arrows indicate orthogonal transfer of an electron and proton, respectively. The proton acceptor for Y_{731}-α2 during its transient oxidation is unknown. The purple arrow in α2 indicates colinear movement of the electron and proton. Y_{356}- and E_{350}-β2 are in the flexible C-terminal tail and are disordered in all crystal structures. There is currently no direct evidence for the involvement of W_{48}-β2 in the radical propagation process, hence indicated by brackets.

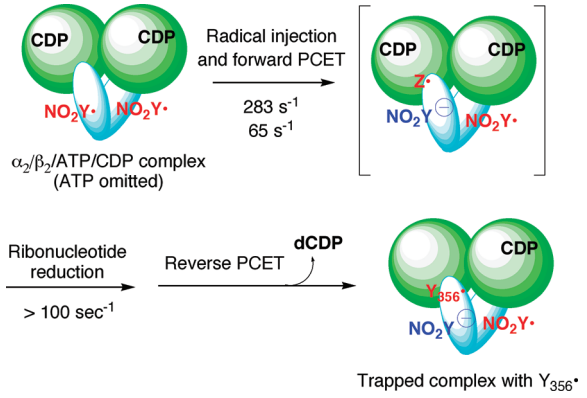

Figure 2. Model for the reaction of $[NO_2Y_{122}^{\bullet}]$-β2 with α2, ATP, and CDP based on rapid kinetics experiments. Reprinted from ref 5. Copyright 2010 American Chemical Society. The green circles represent α and the blue ovals β. ATP, the allosteric effector, is omitted from α for clarity. There are 1.2 $NO_2Y^{\bullet}$ radicals/β2, not 2, as shown in the figure, and their distribution between the two monomers of β is not understood. Any intermediate(s) between the forward PCET and ribonucleotide reduction is (are) designated as $Z^{\bullet}$. Rate constants determined for dCDP and $Y^{\bullet}$ formation (>100 s^{-1}) are limited by the time resolution of the instrument measurement, and these steps likely exhibit biphasic kinetics with rate constants similar to that of the NO_2Y phenolate formation.

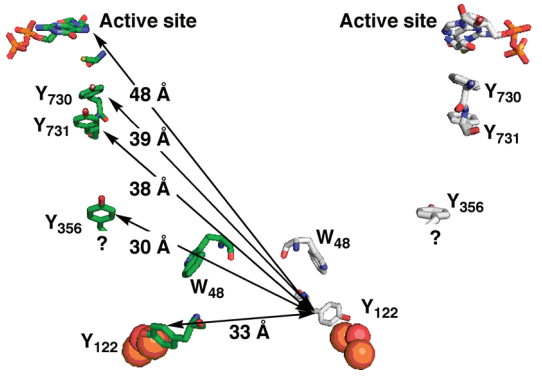

Figure 3. Diagonal distances previously measured in wt and mutant RNRs by PELDOR spectroscopy. Distances shown were determined by PELDOR for $Y_{122}^{\bullet}$–$Y_{122}^{\bullet}$ (33 Å),[16] $Y_{122}^{\bullet}$–$DOPA_{356}^{\bullet}$ (30 Å),[15] $Y_{122}^{\bullet}$–$NH_2Y_{731}^{\bullet}$ (38 Å),[15] $Y_{122}^{\bullet}$–$NH_2Y_{730}^{\bullet}$ (39 Å),[15] and $Y_{122}^{\bullet}$–$N^{\bullet}$ (48 Å; $N^{\bullet}$ is a nitrogen-centered radical observed in the reaction with a mechanism-based inhibitor, 2′-azido-2′-deoxynucleotide diphosphate).[12] The residues constituting a pathway in one $\alpha\beta$ pair are colored in green, and the residues in the second pathway are shown in gray. Y_{356}-β2 is disordered in all crystal structures.

potentials and/or phenolic pK_a values, site-specifically replacing the Y residues in the pathway. The pathway dependence of radical propagation and the redox reactivity of Y_{356}, Y_{731}, and Y_{730} were established, for example, using 3-hydroxytyrosine (DOPA)[10] or 3-aminotyrosine (3-NH_2Y),[11] both of which function as radical traps.

Recently, we reported the results of our studies[5] of the reaction of $[NO_2Y_{122}^{\bullet}]$-β2 (1.2 per β2) with α2/ATP/CDP using pre-steady-state methods, including stopped flow (SF) absorption spectroscopy, rapid freeze quench electron paramagnetic resonance (RFQ EPR) spectroscopy, and rapid chemical quench (RCQ) technology (Figure 2). Kinetic analysis revealed that 0.6 equiv of $NO_2Y^{\bullet}$ was rapidly reduced to 0.6 equiv of NO_2Y phenolate, with rate constants of ~300 and ~100 s^{-1}, and that 0.6 equiv of dCDP and a new radical were produced with similar kinetics. These rate constants show that the reactions are significantly faster than the conformationally gated catalysis by wt RNR,[7] which occurs at 2–10 s^{-1}. The observed nitrophenolate and its stoichiometry indicate that in the reduction of $NO_2Y_{122}^{\bullet}$ the electron transfer is uncoupled from the proton transfer, and the fast rates of its formation indicate that protein conformational gating is also altered. The unusual stoichiometry is indicative of half-site reactivity inherent to the system.[10–13] Additional studies of $NO_2Y_{122}^{\bullet}$-β2 with redox-inactive α2 mutants in the pathway (C_{439}S-α2, Y_{730}F-α2, and Y_{731}F-α2) led to the proposal that the new radical was located on Y_{356} in β2.[5]

The half-site reactivity observed with the $[NO_2Y_{122}^{\bullet}]$-β2α2 experiments suggested that PELDOR spectroscopy would provide an excellent tool to determine the location of the new $Y^{\bullet}$. PELDOR is a pulsed EPR method that allows measurement of weak dipolar interactions between two paramagnetic sites separated by 20–80 Å.[14] The measurements are possible due to the apparent half-site reactivity of the active complex of RNR. Specifically, when DOPA or 3-NH_2Y is site-specifically

incorporated in place of a pathway Y residue, S/E binding to the complex triggers $Y_{122}^{\bullet}$ reduction in one α/β pair and formation of DOPA$^{\bullet}$ or $NH_2Y^{\bullet}$ within the same pair.[15] However, the second α/β pair is unable to trigger a similar reaction, due to a loss of the appropriate signal from the first pair, and thus, $Y_{122}^{\bullet}$ in this second pair remains unchanged. Thus, the distance measured is between $Y_{122}^{\bullet}$ on one α/β pair and the new radical on the second α/β pair across the subunit interface as shown in Figure 3. This method allowed measurement of five distances within the "active" $\alpha2\beta2$ complex, which are within error of those predicted from the docking model.[12,15,16]

In the present paper we describe the use of PELDOR spectroscopy to establish the location of the new Y$^{\bullet}$ generated from incubation of $[NO_2Y_{122}^{\bullet}]$-$\beta2/\alpha2$/CDP and ATP. Unexpectedly, the data suggested that the new Y$^{\bullet}$ is not uniquely located in $\beta2$, but equilibrates onto one or both of the two pathway tyrosines in $\alpha2$. To provide additional support for the interpretation of the PELDOR experiments, $\alpha2$ with 3,5-difluorotyrosine (F_2Y) site-specifically incorporated at position 731 or 730 in $\alpha2$ and $\alpha2$ globally labeled with $[\beta$-$^2H_2]Y$ were examined by RFQ EPR spectroscopy, and the amount of Y$^{\bullet}$ located in $\alpha2$ was quantitated. The results together suggest that Y$^{\bullet}$ is primarily localized (~87%) at Y_{356}-$\beta2$ with ~13% equally distributed between Y_{731} and Y_{730} in $\alpha2$. Using the $[\beta$-$^2H_2]Y$-$\alpha2$ results and data obtained from high-field EPR spectra of the Y$^{\bullet}$ radicals generated with wt-$\alpha2$ and $Y_{731}F$-$\alpha2$, analysis of the temperature-dependent shift of the equilibrium between the radicals in $\beta2$ and $\alpha2$ suggested that the redox potential of Y_{356}-$\beta2$ is ~100 mV lower than that at Y_{731}- and Y_{730}-$\alpha2$. Furthermore, the studies of the trapped Y$^{\bullet}$ radicals by 9 and 140 GHz EPR spectroscopy have provided information on the conformation and electrostatic environment of the pathway Y residues in the active $\alpha2\beta2$ complex.

MATERIALS AND METHODS

$[\beta$-$^2H_2]Y$ was from Cambridge Isotope Laboratory (Andover, MA). EPR tubes for 9 GHz spectroscopy (quartz, o.d. = 4 mm, i.d. = 3.2 mm) were from Wilmad Labglass (Vineland, NJ). EPR tubes for 140 GHz spectroscopy (silica, o.d. = 0.55 mm, i.d. = 0.40 mm) were from Optic Fiber Center Inc. (New Bedford, MA). 2,6-Difluorophenol and 3-nitrotyrosine (NO_2Y) were purchased from Sigma-Aldrich. Isopropyl β-D-thiogalactopyranoside (IPTG) and dithiothreitol (DTT) were from Promega. 3,5-Difluorotyrosine (3,5-F_2Y) was synthesized from 2,6-fluorophenol, sodium pyruvate, and ammonium acetate using tyrosine phenol lyase as described previously.[17] The purifications of wt-$\alpha2$[18] (2200−2700 (nmol/min)/mg), $Y_{731}F$-$\alpha2$,[18] $[3,5\text{-}F_2Y_{730}]$-$\alpha2$[19] (1200−1300 (nmol/min)/mg at pH 7.6), $[3,5\text{-}F_2Y_{731}]$-$\alpha2$[19] (1300−1500 (nmol/min)/mg at pH 7.6), and $[NO_2Y_{122}]$-$\beta2$[20] have previously been described. The concentrations of wt-$\alpha2$ and mutant $\alpha2$ subunits were determined using $\varepsilon_{280\ nm}$ = 189 $mM^{-1}\ cm^{-1}$.[21] The concentrations of $[NO_2Y_{122}]$-$\beta2$ and apo-$[NO_2Y_{122}]$-$\beta2$ were determined using $\varepsilon_{280\ nm}$ = 131 and 120 $mM^{-1}\ cm^{-1}$, respectively.[22]

Determination of the Distance between Y$^{\bullet}$ and $NO_2Y^{\bullet}$ by PELDOR Spectroscopy. Samples for the PELDOR experiments were prepared by the RFQ method as described previously[5] using an Update Instruments 1019 syringe ram unit equipped with three syringes and a model 715 syringe ram controller. Fe(II)-preloaded $[NO_2Y_{122}]$-$\beta2$ (300 μM, 5 Fe(II) atoms/$\beta2$, 150 μL) in anaerobic buffer A [50 mM HEPES (pH 7.6) containing 5% (w/v) glycerol] from one syringe was mixed with an equal volume of buffer A with O_2 (1.3 mM, saturated at 25 °C) and CDP (3 mM) from another syringe and aged for 0.17 s at 25 °C. This solution (300 μL) was then mixed with 150 μL of a solution containing wt-$\alpha2$ or $Y_{731}F$-$\alpha2$ (300 μM), ATP (9 mM), EDTA (3 mM), and $MgSO_4$ (45 mM) in buffer A from the third syringe. The final reaction mixture contained 100 μM $[NO_2Y_{122}]$-$\beta2$, 100 μM $\alpha2$, 3 mM ATP, 1 mM CDP, 1 mM EDTA, and 15 mM $MgSO_4$ in buffer A. The reaction mixture was incubated for 8−570 ms, sprayed into a funnel containing liquid isopentane at −143 ± 3 °C, and then packed into an EPR tube.

PELDOR spectra were recorded at 5 K using a Bruker ELEXSYS E580 X-band spectrometer and a dead-time free four-pulse DEER sequence.[23] $\pi/2$ and π pulses on the detection frequency were 16 and 32 ns, respectively, and the π pulse on the pump frequency was typically 32 ns [τ (spacing between the $\pi/2$ and π pulses) = 128 ns, T = 5 K, 24−48 h acquisition time]. The data were analyzed using DeerAnalysis 2009 software.[24] To extract the modulation frequency, a monoexponential decay function was fit and subtracted from each curve. The resulting oscillation curve was analyzed using the Tikhonov regularization procedure.[25] The regularization parameter, α term, was determined by the L-curve criterion.[24,25]

Determination of the EPR Spectrum of $Y_{356}^{\bullet}$ at 140 GHz. All reactions were performed by hand-mixing at room temperature (20 ± 2 °C). Apo-$[NO_2Y_{122}]$-$\beta2$ (0.4 mM) in O_2-saturated 50 mM HEPES (pH 7.6, 10 μL) was mixed with 2 μL of 10 mM Fe(II) in 5 mM HNO_3, incubated for ~5 s, and then mixed with an equal volume of 0.34 mM wt-$\alpha2$ or $Y_{731}F$-$\alpha2$, 6 mM ATP, and 2 mM CDP in 2× assay buffer. The final solution contained 170 μM $[NO_2Y_{122}]$-$\beta2$, 170 μM wt-$\alpha2$ or $Y_{731}F$-$\alpha2$, 3 mM ATP, and 1 mM CDP in assay buffer. The sample was drawn into an EPR sample tube by capillary action to a height of >2 mm and loaded into the side-coupled TE_{011} cylindrical resonator of the EPR probe, which was then inserted into a cryostat maintained at 70 K by liquid He. The sample was frozen in the cryostat within 15 s of the second mixing by a stream of cold He gas. The 140 GHz pulsed EPR spectra were recorded at 70 K on a home-built spectrometer[26,27] using a $\pi/2-\pi$ spin-echo sequence[28] with typical $\pi/2$ and π pulse lengths of 32 and 64 ns, respectively, and a τ, the time between $\pi/2$ and π pulses, of 200 ns.

Investigation of Y$^{\bullet}$ Distribution in $\alpha2$ Using $[3,5\text{-}F_2Y_{731}]$-$\alpha2$ and $[3,5\text{-}F_2Y_{730}]$-$\alpha2$. The reactions were performed at 25 °C as described above for the PELDOR sample preparation except that $[NO_2Y_{122}^{\bullet}]$-$\beta2$ (30 μM) and $[3,5\text{-}F_2Y_{731}]$-$\alpha2$ or $[3,5\text{-}F_2Y_{730}]$-$\alpha2$ (30 μM) were used. The reactions were freeze-quenched at 60 ms and packed into EPR tubes. Continuous wave EPR (CW-EPR) spectra were recorded on a Bruker ESP 300 X-band spectrometer equipped with a quartz finger Dewar filled with liquid N_2. EPR parameters were a microwave frequency of 9.34 GHz, a power of 30 μW, a modulation amplitude of 1.5 G, a modulation frequency of 100 kHz, a time constant of 5.12 ms, a scan time of 41.9 s, and a conversion time of 20.48 ms. EPR spin quantitation was carried out using $Cu(II)SO_4$ as a standard.[29] All EPR spectral simulations were carried out using EasySpin software.[30]

Expression and Purification of $[\beta$-$^2H_2]Y$-$\alpha2$. *E. coli* DH10B cells transformed with pTrc−*nrdA*[11] were grown at 37 °C in a previously described amino acid (Glu, Gln, Asp, Asn, Lys, Val, Arg, Leu, His, Ile, Ala, Pro, Trp, Gly, Met, Thr, Ser, 0.2 g/L) enriched GMML[20] supplemented with 1 mM $[\beta$-$^2H_2]Y$ and 100 mg/L ampicillin. $\alpha2$ expression was induced at OD_{600} = ~0.8 by addition of 1 mM IPTG. The growth was continued for another 4 h, and the cells were harvested by centrifugation (4000g, 10 min), yielding 5 g/L cell paste. $[\beta$-$^2H_2]Y$-$\alpha2$ was then purified using a previously described procedure[18] with a yield of ~5 mg/g of cell paste. To determine the extent of $[\beta$-$^2H_2]Y$ incorporation, the purified protein was digested by L-1-tosylamido-2-phenylethyl chloromethyl ketone treated porcine trypsin (Sigma), and the peptides were analyzed by LC−MS at the Koch Institute at the Massachusetts Institute of Technology (MIT; see the Supporting Methods and Figure S1 in the Supporting Information for details). In the nonlabeled wt-$\alpha2$ sample, a doubly charged peptide with m/z

529.76 ± 0.03 was eluted at 11−12 min (Figure S1A), which agrees with m/z 529.77 for an expected tryptic peptide fragment (TLYYQNTR) containing Y_{731}- and Y_{730}-α2. The peptide sequence was further confirmed by tandem MS. In the [β-$^2H_2$]Y-α2 sample, a peptide with m/z 531.77 ± 0.05 and a small signal with m/z 529.77 were observed at the same retention time (11−12 min). On the basis of the relative intensities of these peaks in the [β-$^2H_2$]Y-α2 sample, the [β-$^2H_2$]Y incorporation was estimated to be >92%.

Investigation of the Y• Distribution in α2 Using [β-$^2H_2$]Y-α2. The reactions were carried out as described above for the PELDOR sample preparation at 25 °C except that [NO_2Y_{122}•]-β2 (30 μM) and [β-$^2H_2$]Y-α2 (30 μM) were used. The reactions were freeze-quenched at 12, 24, 60, or 115 ms and packed into EPR tubes. The CW-EPR spectra were recorded at 77 K and 9 GHz as described above. The amount of [β-$^2H_2$]Y• was quantitated as described in the Results. The EPR spectral simulations in the analysis were carried out using EasySpin software.[30]

Investigation of the Temperature-Dependent Distribution of the Y• Radicals in α2 Using [β-$^2H_2$]Y-α2. The reactions were carried out at 5, 15, 25, or 37 °C as described above for the PELDOR sample with the following modifications: Fe(II)-preloaded [NO_2Y_{122}]-β2 (90 μM, 5 Fe(II) atoms/β2, 150 μL) in anaerobic buffer A from one syringe was mixed with an equal volume of buffer A with O_2 (2.0, 1.6, 1.3, and 1.0 mM at 5, 15, 25, and 37 °C, respectively) and CDP (3 mM) from the second syringe and aged for 2, 0.2, 0.16, and 0.06 s for the reactions at 5, 15, 25, and 37 °C, respectively. This solution (300 μL) was then mixed with 150 μL of a solution containing [β-$^2H_2$]Y-α2 or α2 (90 μM), ATP (9 mM), EDTA (3 mM), and $MgSO_4$ (45 mM) in buffer A from the third syringe. The final reaction mixture contained 30 μM [NO_2Y_{122}]-β2, 30 μM α2, 3 mM ATP, 1 mM CDP, 1 mM EDTA, and 15 mM $MgSO_4$ in buffer A. The reaction was incubated for 12, 24, 60, or 115 ms at 37, 25, 15, and 5 °C, respectively, sprayed into a funnel containing liquid isopentane at −143 ± 3 °C, and then packed into an EPR tube. The CW-EPR spectra were recorded at 77 K and 9 GHz and analyzed as described above.

The redox potential difference ($\Delta E°$) between Y_{356}-β2 and $Y_{731/730}$-α2 was determined from the observed amounts of [β-$^2H_2$]Y• using the following equation:

$$\log([\beta\text{-}^2H_2\text{-}Y^\bullet]/[Y_{356}^\bullet]) = (\Delta E°F/R)(1/T) \quad (1)$$

where F is the Faraday constant, R is the ideal gas constant, and T is the temperature (K). Details of the analysis, including the method of [β-$^2H_2$]Y• quantitation, are described in the Results.

RESULTS

Optimization of Sample Preparation for PELDOR Experiments. Our previous PELDOR experiments with DOPA•[15] and $NH_2Y^\bullet$ (E. C. Minnihan and J. Stubbe, unpublished results) generated at position 356 in β2 in the reaction with CDP/ATP/α2 gave rise to the diagonal distance from Y_{122}• of 30 Å (Figure 3) in both cases. These results suggest that the PELDOR method would provide evidence for the location of the new Y•, generated when [NO_2Y_{122}•]-β2 is incubated with α2, CDP, and ATP. Optimization was required for the sample preparation to obtain reproducible, analyzable spectra with a good ratio of signal to noise (S/N). An important variable was the method of freezing. Previously, all of our experiments were carried out with "hand-quenching" of samples in liquid nitrogen,[12,15,16] that is, slow freezing. However, in the current experiments the new radical(s) is (are) generated on a millisecond time scale, requiring RFQ methods to trap them. Thus, we compared the results of the hand quench (red trace) and RFQ (blue trace) methods as shown in Figure S2A in the Supporting Information. In both sets of samples the concentration of glycerol was 5%. Subtraction of the monoexponential echo decay function from the observed spectra and fitting by the Tikhonov regularization procedure[25] gave the results shown in Figure S2B. The modulations were markedly improved by the RFQ method or by addition of glycerol (Figure S2A, yellow trace) to the hand-quenched sample. This observation is consistent with previous studies that have established that the RFQ method minimizes protein aggregation problems.[31] A second variable is the spin/protein concentrations that were varied from 50 to 200 μM (total radical). The results are shown in Figure S2C. A 100 μM concentration was chosen to minimize intermolecular dipolar couplings and retain an excellent S/N ratio (Figure S2D). Finally, the glycerol concentration was optimized. Previously, the effects of glycerol concentrations (0−40%) on hand-quenched samples were investigated to measure Y•−Y• distances in *E. coli*[16] and mouse[32] β2, in which some glycerol (5%) was required to prolong the T_2 spin relaxation, while higher concentrations (10−40%) slowed T_1, requiring longer data acquisition times.[32] Similar effects were observed in the current study. In addition, the rate constant for the pathway Y• formation slowed at glycerol concentrations higher than 10% (w/v), and the RFQ sample packing became very difficult due to the stickiness of the frozen solution at glycerol concentrations of ∼30%. Thus, all samples for PELDOR measurements were prepared by the RFQ method with a protein (spin) concentration of 0.1 mM and glycerol concentration of 5%.

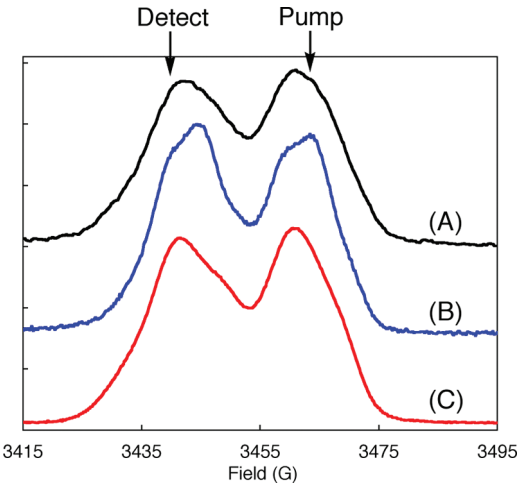

Figure 4. Spin-echo-detected 9 GHz EPR spectrum of the reaction of [NO_2Y_{122}•]-β2 with α2/ATP/CDP rapidly freeze quenched at 24 ms and recorded at 5 K (A, ∼34% trapped Y• and ∼66% $NO_2Y^\bullet$) and at 80 K (B, only trapped Y• is observable). (C) Absorption spectrum of [NO_2Y_{122}•]-β2 alone at 5 K.

Investigation of the Location of Pathway Y• Radicals by PELDOR Spectroscopy. The X-band (9 GHz) spin-echo-detected absorption spectrum of the reaction between [NO_2Y_{122}•]-β2 and wt-α2/CDP/ATP with RFQ at 24 ms is shown in Figure 4 (black trace at 5 K and blue trace at 80 K). The visible doublet spectra arise from the hyperfine coupling (hfc) to one of the two β methylene protons (β-^{1}H atoms) of Y or NO_2Y. The absorption EPR spectrum of the same sample at 80 K reveals only the new Y• (blue trace) as at this temperature $NO_2Y^\bullet$ is not visible due to its faster relaxation properties resulting from its proximity to the diferric cluster. The $NO_2Y^\bullet$ (red trace) in

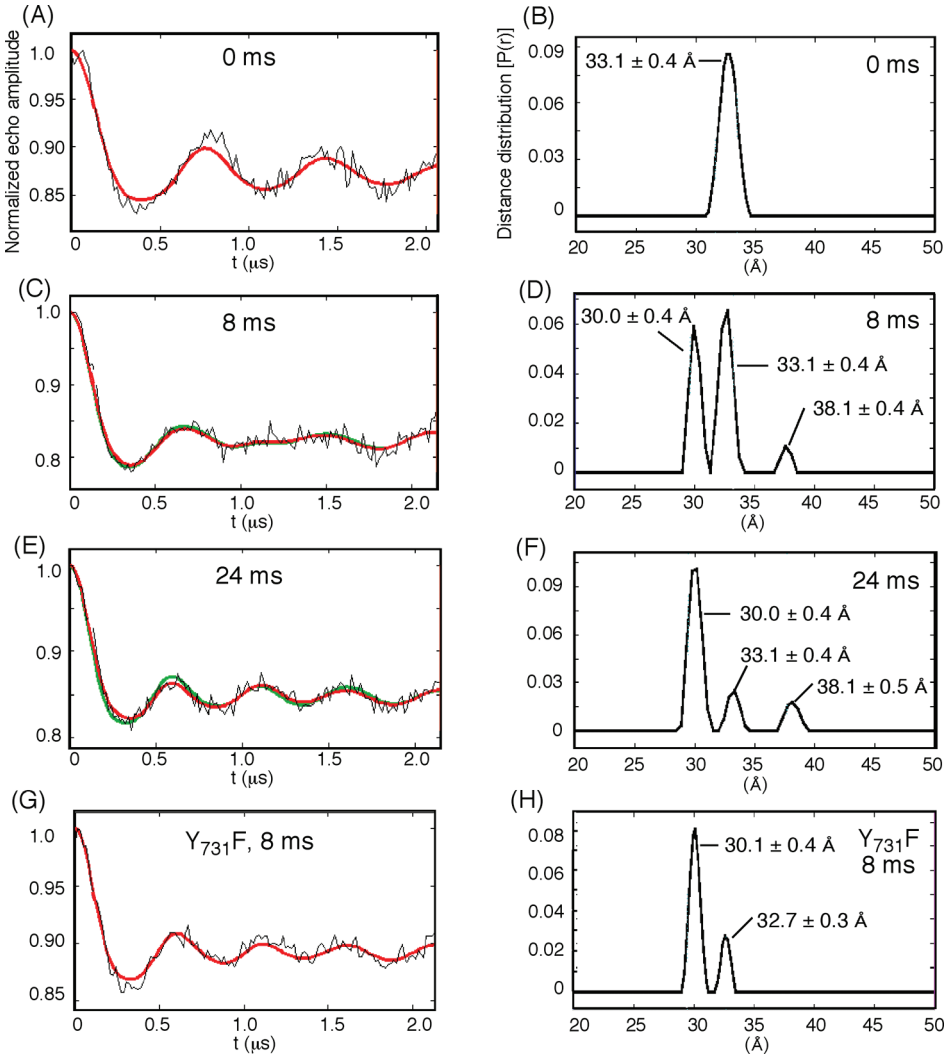

Figure 5. Left column: normalized four-pulse DEER oscillations at 5 K for $[NO_2Y_{122}^{\bullet}]$-β2 alone (A), the $[NO_2Y_{122}^{\bullet}]$-β2/wt-α2/ATP/CDP reaction freeze-quenched at 8 ms (C) and 24 ms (E), and the $[NO_2Y_{122}^{\bullet}]$-β2/Y_{731}F-α2/ATP/CDP reaction freeze-quenched at 8 ms (G). The overlaid red lines are fits using the Tikhonov regularization procedure.[25] Green lines in (C) and (E) are fits without the 38 Å feature. Right column: distance distributions obtained from the analysis of the spectra in the left column. While the relative populations of the 30 and 33 Å peaks changed when Y_{731} was replaced with F, its significance is currently unknown as multiple factors, such as the fitting quality and the relaxation properties of the radicals, might contribute to the altered ratio.

β2 alone at 5 K is shown. A comparison of blue and red spectra reveal extensive overlap, and thus, the pump (P) and detection (D) frequencies for data acquisition were chosen to be at about the peak maxima separated by 60 MHz.[16] Figure 5A shows the echo modulation trace observed for $[NO_2Y_{122}^{\bullet}]$-β2 alone after subtraction of a monoexponential signal decay function. The modulation frequency of this spectrum is indicative of the distance between two $NO_2Y_{122}^{\bullet}$ radicals in β2 (Figure 3). Analysis of this trace using the distance-domain Tikhonov regularization procedure[25] resulted in the distance distribution profile shown in Figure 5B and a distance of 33.1 ± 0.4 Å. The error is based on the peak width at half-height from three different sample preparations. Similar experiments with RFQ-prepared wt-β2 samples with 5% glycerol gave improved fits with a distance of 33.2 ± 0.4 Å (Figure S2B, Supporting Information). The poorer fit of the data with $[NO_2Y_{122}^{\bullet}]$-β2 alone relative to wt-β2 alone may be associated with the presence of excess Fe(III) resulting from the in vitro cluster assembly of $[NO_2Y_{122}^{\bullet}]$-β2, which is not present in wt-β2 assembled in vivo. The observed distance is consistent with the distance between the center of the aromatic rings of two NO_2Y_{122} residues in the β2 dimer observed in the crystal structure of this mutant (32.8 Å)[5] and the $Y_{122}^{\bullet}$−$Y_{122}^{\bullet}$ distance in wt-β2 previously determined by PELDOR (33.1 ± 0.2 Å).[16]

To measure the distance between the trapped $Y^{\bullet}$ and $NO_2Y_{122}^{\bullet}$, the reaction with $[NO_2Y_{122}^{\bullet}]$-β2/wt-α2/ATP/CDP was freeze-quenched at 8 or 24 ms, where 21% ± 3% and 34% ± 4% of $NO_2Y^{\bullet}$ was converted into the pathway $Y^{\bullet}$, respectively, determined by X-band CW-EPR spectroscopy (Figure S3, Supporting Information). The observed echo modulation frequency exhibited time-dependent changes from 8 to 24 ms (compare parts C and E of Figure 5), indicating a transformation of $NO_2Y_{122}^{\bullet}$ to the new radical. The distance distribution profiles shown in Figure 5D,F reveal disappearance of the signal at 33 Å, the $NO_2Y_{122}^{\bullet}$−$NO_2Y_{122}^{\bullet}$ distance, and appearance of two new features at 30 and 38 Å. The distance of 30.0 ± 0.4 Å is within the

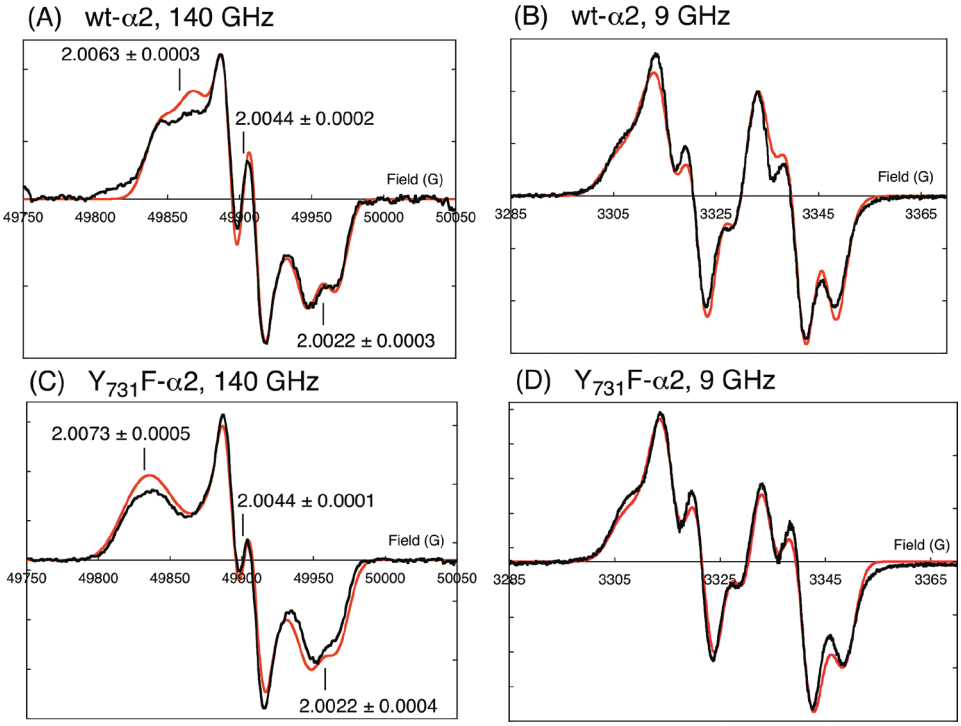

Figure 6. EPR spectra at 140 and 9 GHz of pathway Y• radicals observed in the wt-α2 and Y_{731}F-α2 reactions. The reactions were carried out at room temperature with 170 μM wt- or Y_{731}F-α2, 170 μM [NO_2Y_{122}•]-β2, 3 mM ATP, and 1 mM CDP and freeze-quenched in the cryostat after ~15 s. The 140 and 9 GHz spectra for each reaction were simulated (red traces) using the same set of parameters (Table 1) as described in the text. The *g* values determined by the simulation are indicated in (A) and (C).

error of the distance previously observed for DOPA• at position 356 in β2 (30.6 ± 0.5 Å)[15] and that recently measured for NH_2Y• at position 356 in β2 (30.2 ± 1.6 Å, E. C. Minnihan and J. Stubbe, unpublished results) and is consistent with our previous assignment of the predominant species as Y_{356}•.

The unexpected small signal at 38 Å (Figure 5D,F) was observed in 10 different sample preparations quenched at 8, 24, 120, or 570 ms. The distance is close to those previously observed when [NH_2Y_{731}]-α2 and [NH_2Y_{730}]-α2 were used to generate NH_2Y• at position 731 in α2 (38.1 ± 1.2 Å) and position 730 in α2 (38.7 ± 1.8 Å),[15] respectively. The peak area associated with this feature ranged from 8% to 15% of the 30 Å feature. As one test of the "reality" of the 38 Å feature, the Tikhonov regularization analysis was carried out by limiting the distance distribution range from 20 to 36 Å. The results of these analyses are shown in Figure 5C,E (green traces), which are very similar to those of the analyses with the full distance range (20−50 Å). Thus, the analysis itself cannot establish the reality of the 38 Å peak. However, the peak was reproducibly observed in all samples regardless of the choice of the Tikhonov regularization parameter, α, or the position of the background fitting, suggesting that the peak is not an artifact of the data analysis.

If the 38 Å feature is associated with the Y• radical(s) in α2, the 38 Å distance would not be observable in a PELDOR experiment using Y_{731}F-α2 in place of wt-α2, which would localize the radical at Y_{356}-β2. It is important to point out, however, that the Y_{356}• observed in this mutant reaction is generated in the forward radical propagation and not the back radical propagation as in the wt-α2 reaction. The reaction was quenched at 8 ms, and 25% ± 2% of the total radical was trapped as the pathway Y•. The PELDOR experiments and analyses on four independently prepared samples quenched at 8 or 24 ms revealed only two distances: 30 and 33 Å.[33] Although the fits are not as good as those for wt-α2 experiments (compare parts C and E with part G of Figure 5), they provide support for our proposal that the 38 Å distance observed in wt-α2 reactions is associated with Y• radicals at position 731/730 in α2.

High-Field EPR (HF-EPR) of Y_{356}•. As described subsequently, further studies to obtain evidence for new radical delocalization in α2 required EPR spectral simulations. Thus, the *g* values and hfc's for Y_{356}• were determined by simulation of EPR spectra at 9 and 140 GHz. As this is the first Y• observed on the pathway, determination of these parameters is important in understanding the protein environment, its H-bonding interactions and electrostatic environment, and the conformation of Y_{356}-β2 in the active $\alpha2\beta2$ complex. In addition, determination of the *g* values and hfc parameters will also allow us to compare them with those measured for NH_2Y_{356}• and $DOPA_{356}$• and offer one method to evaluate the extent of the perturbations caused by the presence of an NH_2 or OH group at the ortho position of the phenol of these amino acids.

Y_{356}• was generated with either wt- or Y_{731}F-α2 and [NO_2Y_{122}•]-β2/CDP/ATP by hand mixing/freezing.[5] In the Y_{731}F-α2 case, only Y_{356}• is observable in addition to NO_2Y_{122}•, while in the wt-α2 case, the trapped radical is composed of Y_{356}• and up to 15% additional radical species. We have previously reported that the pulsed EPR method can filter the signal of radicals in α2[34] and at position 356 in β2 (unpublished results) from that of Y_{122}• in β2 when the electron spin-echo spectrum is recorded at 70 K. At this temperature and 140 GHz, we verified that the signal associated with NO_2Y_{122}•, adjacent to the diferric cluster, is not observable. The resulting absorption spectra for

Table 1. Hfc's (MHz) Used in the EPR Simulations

position	nucleus	A_{xx}	A_{yy}	A_{zz}
3,5-$F_2Y_{730}^{\bullet}$ [a,b]	β-^{1}H[e,f]	63	63	63
	$^{19}F_a$[e,g]	−15	−3	151
	$^{19}F_b$[e,g]	15	3	−151
3,5-$F_2Y_{731}^{\bullet}$ [a,b]	β-^{1}H[e,f]	40	40	40
	$^{19}F_a$[e,g]	−15	−3	157
	$^{19}F_b$[e,g]	15	3	−157
[β-$^2H_2$]$Y^{\bullet}$ [a,b]	3,5-^{1}H[h]	27	8	19
	β-^{2}H[e,f]	8	8	8
pathway $Y^{\bullet}$ in the wt-α2 reaction[a,c]	3,5-^{1}H[h]	26	4	18
	β-^{1}H[e]	61	52	54
pathway $Y^{\bullet}$ in the $Y_{731}F$-α2 reaction[a,d]	3,5-^{1}H[h]	26	4	18
	β-^{1}H[e]	54	52	54

[a] The intrinsic EPR line width of 17 MHz was used. Hfc's for 2,6-^{1}H and one of the two β-^{1}H atoms or β-^{2}H atoms were not included in the simulation as they are significantly smaller than the intrinsic EPR line width. [b] g values of 2.0063, 2.0044, and 2.0022 were used on the basis of the assumptions described in the text. [c] g values of 2.0063, 2.0044, and 2.0022 were used. [d] g values of 2.0073, 2.0044, and 2.0022 were used. [e] Hyperfine tensor axes were assumed to be colinear with the **g** tensor axes.[17,35] [f] Hfc's for β-^{1}H or β-^{2}H were assumed isotropic on the basis of the reported small anisotropy for this position.[35] [g] A_{xx} and A_{yy} for ^{19}F were chosen on the basis of the previous characterization of 3-$FY^{\bullet}$.[17] [h] Euler angles of $[\alpha, \beta, \gamma] = [\pm 22°, 0°, 0°]$[35] were used.

wt- or $Y_{731}F$-α2 were obtained and converted to the first-derivative spectra as shown in parts A and C, repectively, of Figure 6. The corresponding 9 GHz CW-EPR spectra were also acquired by hand quenching, and the $NO_2Y_{122}^{\bullet}$ spectrum was removed by subtraction[5] (Figure 6B,D).

Analysis of the spectra at these two frequencies required a simulation strategy in which the constraints posed by the spectra at the different frequencies were determined, as far as possible, and then combined to find a global solution. The simulation of the 9 GHz spectra was attempted first by assuming one large isotropic hfc for one of the β-^{1}H atoms, a line-broadening factor of 11 MHz associated with the unresolved hfc's, and anisotropic hfc's for the 3,5-^{1}H atoms of the ring ($[A_{xx}, A_{yy}, A_{zz}] = [27, 8, 19]$ MHz), almost invariable in $Y^{\bullet}$ radicals observed in biological systems.[35] Because the X-band EPR spectra are rather insensitive to g values, the values for $Y_{122}^{\bullet}$ in wt-β2 (2.009, 2.0046, and 2.0023) were initially used. The 140 GHz spectra were then simulated using the parameters obtained from the 9 GHz simulations. The deviation in the g values was immediately observed, and the values were adjusted. The hfc's for β-^{1}H were also varied, and line-broadening factors associated with the width of the Gaussian distribution of g values (g strain) were introduced. The simulations were repeated between the spectra at 140 and 9 GHz until the square deviations at both frequencies were minimized. The results of the final simulations are shown in Figure 6 (red) and the parameters summarized in Table 1. While the simulation reproduced the $Y^{\bullet}$ spectrum from the experiments with $Y_{731}F$-α2, the simulation of the wt-α2 reaction at 140 GHz did not reproduce the shoulder feature at 49800−49830 G, suggesting the presence of an additional minor component(s). This deviation was not detectable at 9 GHz, and thus, the additional species likely has perturbed g values with hfc's similar to those of the predominant species. The major species in the wt-α2 reaction has a g_{xx} value of 2.0063, distinct from the value of 2.0073 found in the $Y_{731}F$-α2 reaction (Table 1). $Y_{356}^{\bullet}$ is the predominant species in both reactions on the basis of the PELDOR data and other experiments described subsequently. The protein environments of the two radicals are identical except that the OH of Y_{731} is replaced with a H in the mutant. The g_{xx} values of $Y^{\bullet}$ radicals in biology have been shown to be sensitive to their H-bonding/electrostatic environments, with values varying between 2.006 and 2.009, with the smaller values associated with H bonding.[35−38] Thus, the current observation is intriguing in terms of differences in H bonding.

Probing the Radical Distribution at Positions 731 and 730 in α2 Using [3,5-F_2Y_{731}]- and [3,5-F_2Y_{730}]-α2 Mutants. Two types of experiments were carried out to provide further support that the new radical is composed of three $Y^{\bullet}$ radicals, with ∼10% delocalized at Y_{731}- and Y_{730}-α2. Detection of small amounts of $Y^{\bullet}$ in α2 in the presence of $NO_2Y_{122}^{\bullet}$ and $Y_{356}^{\bullet}$ is challenging as the EPR spectra of all the species overlap (Figure 4). We have recently evolved a tRNA/tRNA synthetase pair that can site-specifically incorporate a series of F_nY (n = 2 or 3) into either β2 or α2.[19] RNRs with 3,5-F_2Y, for example, in place of Y_{122}-β2, Y_{731}-α2, or Y_{730}-α2 have been prepared. Our studies with 3-$FY^{\bullet}$ [17] and 3,5 $F_2Y^{\bullet}$ [19] at residue 122 in β2 reveal that these radicals exhibit characteristic splitting patterns with couplings of ∼54 MHz associated with a β-^{1}H, similar to the hfc of a β-^{1}H in $Y_{122}^{\bullet}$. In addition, strong couplings of 150−180 MHz associated with the ^{19}F nucleus are also readily detected in the low-field and high-field regions of the EPR spectrum, as they appear outside the contribution from the features associated with $Y^{\bullet}$ radicals. Thus, 3,5-$F_2Y^{\bullet}$ is detectable even in the presence of $NO_2Y^{\bullet}$ and other pathway $Y^{\bullet}$ radicals. 3,5-F_2Y was chosen as a probe to look for radical delocalization in α2 because its redox potential is within ±30 mV of that of Y between pH 6.5 and pH 8.0 if we assume that the pK_a of this residue is not significantly perturbed in the protein environment.[17] Our previous studies using NO_2Y as a reporter on pK_a perturbation at positions 731 and 730 in α2 have shown this to be the case (pK_a perturbation of ≤1.2 pH units).[20]

The reactions of [$NO_2Y_{122}^{\bullet}$]-β2 with [3,5-F_2Y_{731}]-α2 or [3,5-F_2Y_{730}]-α2 in the presence of ATP and CDP were therefore carried out at 25 °C, pH 7.6, with rapid freeze quenching at 60 ms. If we assume that the kinetics of radical propagation with these mutants are similar to that with wt-α2, a reasonable assumption based on the measured specific activities of these mutants (60−80% of wt-α2 at pH 7.6[19]), 50% of the initial $NO_2Y^{\bullet}$ should be reduced and a corresponding amount of pathway radicals should be formed (Figure S4, Supporting Information). Figure 7 shows the EPR spectra of the quenched reactions with [3,5-F_2Y_{731}]-α2 or [3,5-F_2Y_{730}]-α2 after subtraction of the $NO_2Y^{\bullet}$ spectrum (50% of the total radical). Immediately apparent are the characteristic features on the high- and low-field sides of each spectrum, indicative of the hyperfine splitting associated with ^{19}F atoms and a β-^{1}H (see the brackets in Figure 7). The feature indicated by and asterisk in Figure 7D is unidentified and is also observed in the reaction with wt-α2. Despite the overlap of most of the spectrum of each 3,5-$F_2Y^{\bullet}$ with that of the predominant $Y_{356}^{\bullet}$, each $F_2Y^{\bullet}$ spectrum was simulated to reproduce its low-field and high-field features. The g values [(g_{xx}, g_{yy}, g_{zz}) = (2.0063, 2.0044, 2.0022)] were chosen on the basis of the HF-EPR spectra for the trapped $Y^{\bullet}$ observed in wt-α2 (Figure 6A). Variation of the g_{xx} values ranging from 2.0091 (wt-$Y_{122}^{\bullet}$) to 2.0063 in the simulation of the 9 GHz spectra showed minimal effect and can therefore be neglected. The hfc's for

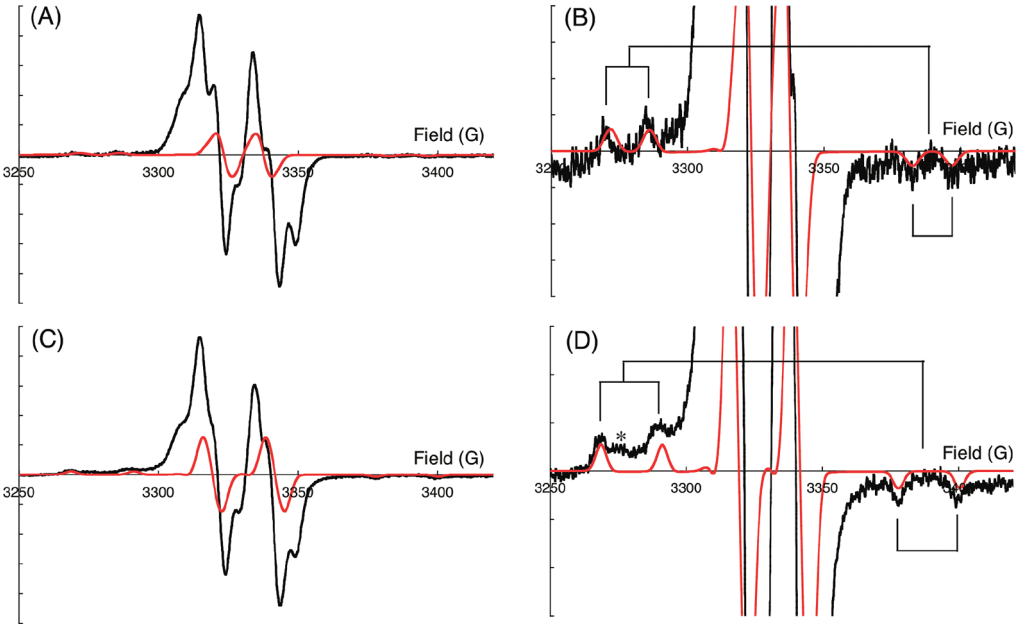

Figure 7. EPR spectra of the pathway radicals formed in the reaction of [3,5-F_2Y_{731}]-α2 (A, B) or [3,5-F_2Y_{730}]-α2 (C, D) with [$NO_2Y_{122}^{\bullet}$]-β2/ATP/CDP quenched at 60 ms (black traces) overlaid with simulated EPR spectra of 3,5-$F_2Y^{\bullet}$ (red traces). The EPR spectrum of $NO_2Y^{\bullet}$ (50% of the total radical) was subtracted from the observed spectrum. (B) and (D) are magnified views of (A) and (C), respectively. The EPR spectral simulations were carried out using the parameters shown in Table 1. Only the low- and high-field doublet features were simulated as described in the text. The asterisk in (D) indicates an uncharacterized signal that has also been observed in the reaction with wt-α2. Brackets in (B) and (D) indicate the hyperfine splitting associated with ^{19}F and β-^{1}H.

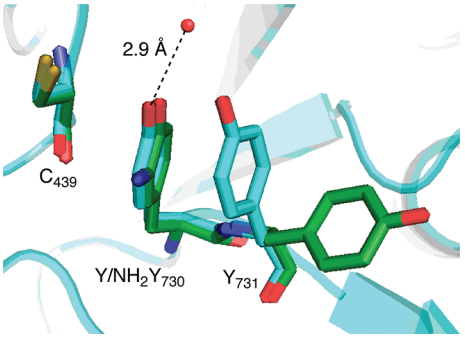

Figure 8. Overlay of X-ray structures of pathway residues in wt-α2 (blue, PDB ID 2X0X)[20] and in one of the three subunits in the asymmetric unit of the crystal structure of [NH_2Y_{730}]-α2 (green, PDB ID 2XO4).[42] A conserved water molecule close to residue 730 is shown along with the distance to the phenol oxygen atom of Y_{730}-α2.

2,6-^{1}H atoms and for the second β-^{1}H are in general smaller than the intrinsic line width (17 MHz) and thus were not included specifically in the simulation. Thus, the key variables in the simulations are the hfc associated with one of the β-^{1}H atoms, assumed to be isotropic, and that associated with the ^{19}F nucleus. The results of the simulations are shown in Figure 7 (red traces), and the hfc's are summarized in Table 1. The hfc's associated with ^{19}F atoms are 157 and 151 MHz for [3,5-F_2Y_{731}]-α2 and [3,5-F_2Y_{730}]-α2, respectively, similar to those previously reported for 3-$FY_{122}^{\bullet}$[17] and 3,5-$F_2Y_{122}^{\bullet}$.[19] The β-^{1}H hfc's are 40 ± 5 and 63 ± 6 MHz for [3,5-F_2Y_{731}]-α2 and [3,5-F_2Y_{730}]-α2, respectively.

The amount of 3,5-$F_2Y^{\bullet}$ was approximated from the simulated spectrum. The signal heights of the doublet features in the simulated and experimental spectra were adjusted (Figure 7B,D) and the double integrals of the two spectra compared. This analysis contains significant error associated primarily with the line-broadening factors (17 ± 4 MHz) used in the simulations, which affected the height of the doublet features. Nevertheless, the analyses of three independent experiments indicate that 3,5-$F_2Y_{731}^{\bullet}$ and 3,5-$F_2Y_{730}^{\bullet}$ accounted for 5% ± 3% and 9% ± 4% of the trapped pathway radicals, respectively. The sum of these values is similar to the intensity of the 38 Å peak (8−15%) observed in the PELDOR experiments. The observation of $F_2Y^{\bullet}$ unambiguously establishes the presence of the radical in α2 at both pathway residues.[39]

The hfc of β-^{1}H reports on different geometries of the tyrosyl side chain within the protein. The isotropic part (A_{iso}) of the hfc for one of the β-^{1}H atoms not only depends on the spin density of the adjacent carbon of the ring system (C1), but also strongly depends on the geometry of the side chain according to $A_{iso} \approx (B_1\rho^{\pi}_{C1}\cos^2\theta)$, where ρ^{π}_{C1} is the π spin density at C1, θ (Figure S5, Supporting Information) is the dihedral angle between the C_β−H bond and the p_z orbital at C1, and B_1 is an empirical constant and is assumed to be 162 MHz.[40] A_{iso} for one of the β-^{1}H atoms of 3,5-$F_2Y_{730}^{\bullet}$ is 63 MHz, while that for the other is not observable and is smaller than the intrinsic line width of ~17 MHz of the spectrum. Using this value, one can calculate $\theta = -70° \pm 6°$ or $10° \pm 5°$ ($\rho_{C1} = 0.41 \pm 0.02$), which is consistent with the conformation of Y_{730}-α2 ($\theta = -67° \pm 4°$) observed in the crystal structures of wt-α2[3,41] and mutant α2.[8,20,42]

A similar analysis for 3,5-$F_2Y_{731}^{\bullet}$ allows calculation of $\theta = 80° \pm 3°$ or $40° \pm 3°$ ($\rho_{C1} = 0.42 \pm 0.02$). Two conformations have been reported for Y_{731} in wt-α2 and mutant α2. The one most frequently found and shown in most renditions of the structure has $\theta = 3° \pm 3°$ (Figure 8, blue structure).[3,41] Recently, however, a second conformation has been reported in our NH_2Y_{730}-α2

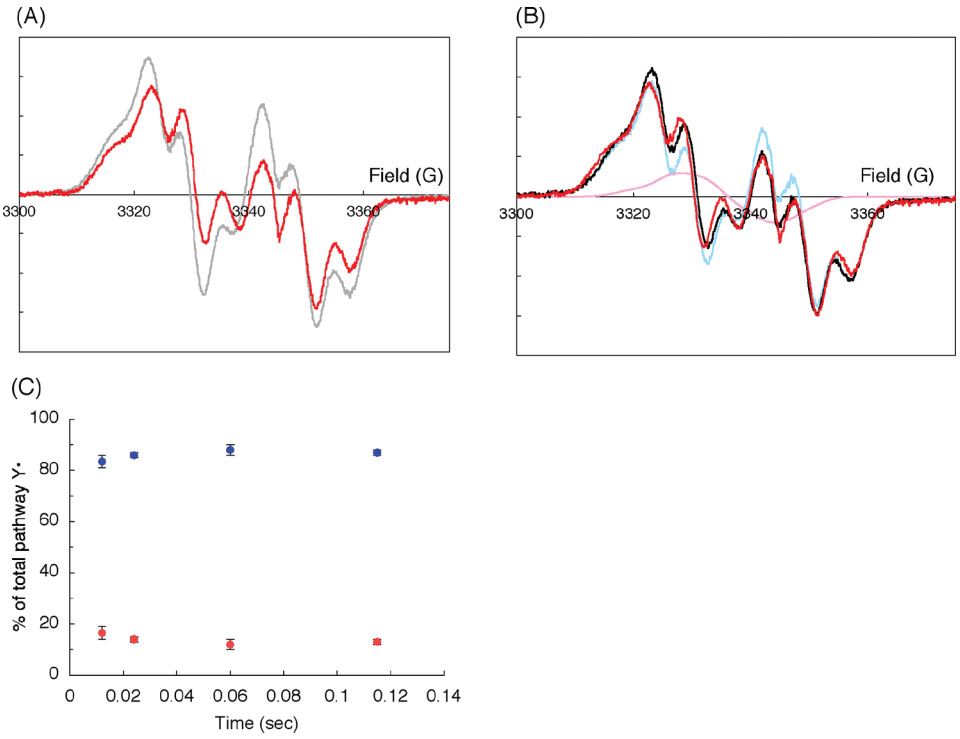

Figure 9. (A) EPR spectrum of pathway $Y^{\bullet}$ radicals observed in the reaction with $[NO_2Y_{122}^{\bullet}]$-β2/$[\beta$-$^2H_2]$Y-α2/ATP/CDP carried out at 25 °C and quenched at 115 ms (red trace). The EPR spectrum observed in the same reaction using nonlabeled α2 is overlaid (gray trace). The $NO_2Y_{122}^{\bullet}$ spectrum (50% of the total radical) was subtracted from the observed spectra in both cases. (B) EPR spectral reconstruction using the spectrum of $Y_{356}^{\bullet}$ observed in the $[NO_2Y_{122}^{\bullet}]$-β2/$[Y_{731}F]$-α2/ATP/CDP reaction (blue, 87%) and that of $[\beta$-$^2H_2]Y^{\bullet}$ simulated using the parameters shown in Table 1 as described in the text (pink, 13%). The sum of the two spectra is shown in the black trace and overlaid with the EPR spectrum of pathway $Y^{\bullet}$ radicals observed in the $[NO_2\ Y_{122}^{\bullet}]$-$\beta$2/$[\beta$-$^2H_2]$Y-$\alpha$2/ATP/CDP reaction freeze-quenched at 115 ms (red trace). (C) Time course of the relative ratios of $Y_{356}^{\bullet}$ (blue) and $[\beta$-$^2H_2]Y^{\bullet}$ (red) at 25 °C determined as described in (B). Each point represents an average of two or three experiments.

crystal structure in one of the three subunits in the asymmetric unit. In this case, $\theta = 82°$ (Figure 8, green structure).[42] The hfc of 3,5-$F_2Y_{731}^{\bullet}$ is most consistent with the latter. This observation suggests that Y_{731}-α2 is flexible and may undergo conformational changes upon complex formation with β2 to catalyze radical propagation. If this conformation is catalytically active, then it has interesting mechanistic implications.

Probing the Radical Distribution in α2 Using $[\beta$-$^2H_2]$Y-α2. As the second approach to obtaining evidence for the $Y^{\bullet}$ distribution over multiple residues, α2 was prepared with $[\beta$-$^2H_2]$Y replacing all Y residues. $[\beta$-$^2H_2]$Y was chosen on the basis of the difference in the gyromagnetic ratios of ^1H and ^2H, which reduces the hfc associated with β-^1H 6.5-fold and collapses the doublet feature of the $Y^{\bullet}$ EPR signal into a broad singlet. Thus, $[\beta$-$^2H_2]Y^{\bullet}$ can be detected as a change in the EPR line shape even though it contributes to only 10−15% of the new $Y^{\bullet}$.

$[\beta$-$^2H_2]$Y was globally incorporated by overexpression of wt-α2 in a defined medium containing $[\beta$-$^2H_2]$Y instead of Y. $[\beta$-$^2H_2]$Y-α2 was purified to homogeneity and had a specific activity of 2300 (nmol/min)/mg, comparable to that of wt-α2. The extent of label incorporation was determined as >92% by LC−MS analysis of peptides from trypsin digestion (see the Supporting Methods and Figure S1 in the Supporting Information for details).

The kinetics of the reaction of $[\beta$-$^2H_2]$Y-α2 with $[NO_2Y_{122}^{\bullet}]$-β2/ATP/CDP were studied at 25 °C with quenching at 12−115 ms. Analysis of the EPR spectra involved subtraction of the $NO_2Y^{\bullet}$ spectrum from the observed spectrum using the broad feature at the low-field side of the $NO_2Y^{\bullet}$ spectrum as described previously.[5] The amounts of $NO_2Y^{\bullet}$ reduced and new pathway radical formed were very similar to results previously reported with wt-α2 (Figure S4, Supporting Information). The resulting spectrum of the pathway radicals quenched at 115 ms is shown in Figure 9A (red spectrum) and is distinct from that observed in the reaction with wt-α2 (gray spectrum). Similar spectra were observed at other quench times (Figure S6, Supporting Information).

The amount of $[\beta$-$^2H_2]Y^{\bullet}$ in α2 was quantitated by reproducing the observed EPR spectrum by varying the amount of the $Y_{356}^{\bullet}$ spectrum, from the EPR spectrum of $Y^{\bullet}$ observed in the $Y_{731}F$-α2/$[NO_2Y_{122}^{\bullet}]$-β2/ATP/CDP reaction, and the amount of the $[\beta$-$^2H_2]Y_{730/731}^{\bullet}$ spectrum, from simulations described subsequently. The EPR spectrum of $Y_{356}^{\bullet}$ was assumed to be identical to that observed in the RFQ experiment of the $Y_{731}F$-α2/$[NO_2Y_{122}^{\bullet}]$-β2/ATP/CDP reaction. Although our HF-EPR spectrum at 140 GHz revealed that the $Y_{731}F$ mutation perturbs the g_{xx} value of $Y_{356}^{\bullet}$, this spectral perturbation at 9 GHz is minimal (compare parts B and D of Figure 6). The EPR spectrum of $[\beta$-$^2H_2]Y^{\bullet}$ was simulated using the parameters in Table 1 obtained from the following analysis: The hfc's for β-^2H of $[\beta$-$^2H_2]Y^{\bullet}$ at positions 731 and 730 in α2 were calculated to be 6 and 10 MHz, respectively, assuming that the hfc's simulated for 3,5-$F_2Y^{\bullet}$ radicals are indicative of the $Y^{\bullet}$ conformation in these positions. The simulations with hfc's within this range resulted in very similar spectra (Figure S7, Supporting Information), and therefore, $[\beta$-$^2H_2]Y^{\bullet}$ in α2 was simulated with an A_{iso} of 8 MHz. The g values in the simulations were $[g_{xx}, g_{yy}, g_{zz}]$ = [2.0063,

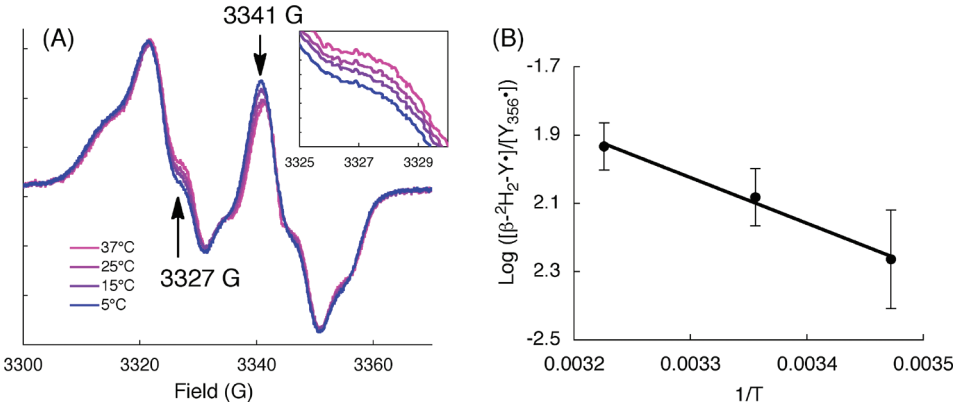

Figure 10. (A) Overlaid EPR spectra of the $[NO_2Y_{122}^{\bullet}]$-β2/$[\beta$-$^2H_2]$Y-α2/ATP/CDP reaction at 5 (blue), 15, 25, and 37 °C (red) without subtraction of the $NO_2Y^{\bullet}$ spectrum. The arrows indicate the change induced by the shift in the temperature. Each spectrum is an average of two or three experiments. The inset is a magnified view between 3325 and 3330 G. (B) $\log([[\beta$-$^2H_2]Y^{\bullet}]/[Y_{356}^{\bullet}])$ vs $1/T$. The $[[\beta$-$^2H_2]Y^{\bullet}]$ values determined for the reactions at 15, 25, and 37 °C were used. At 5 °C, the amount of $[\beta$-$^2H_2]Y^{\bullet}$ could not be quantitated. The line is a linear least-squares fit to eq 1 with $\Delta E^{\circ} = 110$ mV. Each point represents an average of two or three experiments.

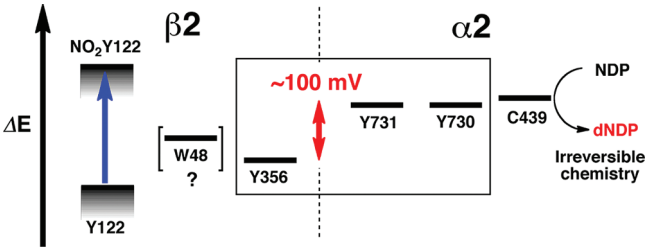

Figure 11. Model of the relative redox potentials of PCET pathway residues in *E. coli* RNR. The box highlights Y_{356}-β2, Y_{731}-α2, and Y_{730}-α2, the $Y^{\bullet}$ radicals observed in the present studies. W_{48}-β2 is in brackets as there is currently no direct evidence for its involvement in the radical propagation process. The range of the redox potential for NO_2Y_{122}, which in solution at pH 7.0 is 210 mV[45] harder to oxidize than Y, is based on the unknown redox potential for Y_{122}, hence the shaded area. The placement of Y_{356} relative to Y_{122} is based on studies with 2,3,5-$F_3Y_{122}^{\bullet}$ (20−100 mV harder to oxidize than Y between pH 6.5 and pH 8.0, assuming no pK_a perturbation by the protein) as the radical initiator where the $Y_{356}^{\bullet}$ is detected.[19].

2.0044, 2.0022], and their variation made little difference as described above for the simulation of 3,5-$F_2Y^{\bullet}$. The resulting simulated spectrum of $[\beta$-$^2H_2]Y^{\bullet}$ was then combined with the $Y_{356}^{\bullet}$ spectrum in appropriate ratios to reproduce the experimentally observed spectra (Figure 9B and Figure S6, Supporting Information). For example, the sum of the $Y_{356}^{\bullet}$ spectrum (blue, 87%) and the simulated $[\beta$-$^2H_2]Y^{\bullet}$ spectrum (pink, 13%) is shown in the black trace in Figure 9B and compared with the spectrum of the pathway radical observed in the reaction with $[\beta$-$^2H_2]$Y-α2 freeze-quenched at 115 ms (red trace). The ratio of the $Y_{356}^{\bullet}$ and simulated $[\beta$-$^2H_2]Y^{\bullet}$ spectra was optimized by minimizing the root-mean-square deviation of the black trace from the red trace.

The EPR spectra of pathway $Y^{\bullet}$ at the other time points (12, 24, 60, and 115 ms) were analyzed in a similar manner (Figure S6, Supporting Information). The pathway $Y^{\bullet}$ was 35% ± 3%, 41% ± 2%, 49% ± 2%, and 50% ± 2% of total radical and the amounts of $[\beta$-$^2H_2]Y^{\bullet}$ were 15% ± 2%, 13% ± 2%, 13% ± 2%, and 13% ± 1% for 12, 24, 60, and 115 ms, respectively, from three independently prepared samples. The errors are associated mainly with the subtraction of the $NO_2Y_{122}^{\bullet}$ spectrum. These observations, with the caveats associated with the assumptions described above, suggest that the amounts of $[\beta$-$^2H_2]Y^{\bullet}$ radicals in α2 are similar over the time course and that 13−15% of the total $Y^{\bullet}$ is distributed in α2 and is in equilibrium with $Y_{356}^{\bullet}$ in β2.

Temperature-Dependent Equilibration between $Y_{356}^{\bullet}$ and $[\beta$-$^2H_2]Y^{\bullet}$ in α2. If $Y_{356}^{\bullet}$-β2, $Y_{731}^{\bullet}$-α2, and $Y_{730}^{\bullet}$-α2 are in equilibrium, the ratio of $Y_{356}^{\bullet}$ to $[\beta$-$^2H_2]Y^{\bullet}$ in α2 should change with temperature, which would allow an estimate of their relative redox potentials. Thus, these experiments were carried out at 5, 15, 25, and 37 °C. To determine the appropriate quenching times for EPR analysis, the kinetics of $NO_2Y^{\bullet}$ reduction in the reaction of $[NO_2Y_{122}^{\bullet}]$-β2/wt-α2/ATP/CDP at these temperatures were studied by SF absorption spectroscopy. In all cases, the kinetics were biphasic and the Arrhenius plot showed a linear correlation (Figure S8, Supporting Information), suggesting that the rate-determining step does not change within this temperature range. These studies also defined the timing of RFQ-EPR experiments so that quenching occurred at >95% completion. Figure 10A shows the EPR spectra of the reactions at 5, 15, 25, and 37 °C without subtraction of the remaining $NO_2Y^{\bullet}$ spectrum. Small changes in the EPR line shape at 3327 and 3341 G are observed (arrows, Figure 10A). These positions are close to the maximum and minimum of the simulated $[\beta$-$^2H_2]Y^{\bullet}$ signal (Figure 9B, pink trace). Thus, the observed changes indicate that increased amounts of $[\beta$-$^2H_2]Y^{\bullet}$ are produced at higher temperatures.

The amounts of $[\beta$-$^2H_2]Y^{\bullet}$ relative to the total pathway radicals were determined as 15% ± 1%, 13% ± 2%, and 10% ± 2% at 37, 25, and 15 °C, respectively, using the method described above. At 5 °C, the amount of $[\beta$-$^2H_2]Y^{\bullet}$ was too small (<8%) for the analysis. A ΔE° of 110 ± 50 mV was calculated from the slope of a plot of $\log([Y_{356}^{\bullet}]/[[\beta$-$^2H_2]Y^{\bullet}])$ vs $1/T$ (Figure 10B).

DISCUSSION

Initiation of deoxynucleotide formation with the hot oxidant $NO_2Y_{122}^{\bullet}$-β2, accompanied by the fortuitous uncoupling of PCET during $NO_2Y_{122}^{\bullet}$ reduction, has allowed for the first time the observation of the three transient $Y^{\bullet}$ radicals in the pathway

(Figure 11). The inability of this RNR to turn over more than once suggests that the predominant radical, identified by our PELDOR experiments, $Y_{356}^{\bullet}$, is unable to reoxidize (directly or through W_{48}-β2) the NO_2Y_{122} phenolate. Thus, the three $Y^{\bullet}$ radicals observed are likely formed during the reverse PCET, subsequent to dCDP formation. These studies have confirmed the original model for this long-range oxidation over 35 Å and have provided us with additional insight into the redox potentials of these three $Y^{\bullet}$ radicals relative to one another and the radical initiator $Y_{122}^{\bullet}$. Furthermore, the EPR analysis has provided us with insights into the H-bonding environment of $Y_{356}^{\bullet}$ and the conformations of $Y_{730}^{\bullet}$ and $Y_{731}^{\bullet}$, which are essential to understanding whether colinear PCET within α2 is feasible.

Thermodynamics of the Problem. We developed three independent strategies, all using the $[NO_2Y_{122}^{\bullet}]$-β2 oxidant, to identify the location of $Y^{\bullet}$ radicals and their distribution in the pathway. PELDOR experiments with wt-α2 and EPR experiments with $[3,5\text{-}F_2Y_{731(730)}]$-$\alpha$2 and $[\beta\text{-}^2H_2]$Y-α2 together revealed that the new radical observed is a composite of three $Y^{\bullet}$ radicals and that 85−90% of the new radical resides at Y_{356} in β2 and that the remaining 10−15% is distributed equally between Y_{731} and Y_{730} in α2. If the observed $Y^{\bullet}$ radicals are in equilibrium, the distribution of 9:1 at 25 °C between β2 and α2 suggests a difference in redox potential of ∼70 mV. The observed temperature dependence of the amounts of these radicals, while of limited scope due to the poor sensitivity of the EPR analysis, supports a redox potential difference between $Y_{356}^{\bullet}$ and $Y_{731}^{\bullet}$ in this range as well, 110 ± 50 mV. In addition, our EPR analysis reveals similar amounts of $3,5\text{-}F_2Y^{\bullet}$ at positions 731 and 730 in α2, indicative of small redox potential differences between these two Y residues in α2. Figure 11 summarizes our current model for this process by fixing the relative redox levels of these three Y residues.

Using a series of β2 mutants with F_nY residues replacing residue Y_{356}, we have previously demonstrated that dCDP production is turned off when the redox potential of F_nY becomes higher than that of Y by 80 mV.[43] Thus, Y_{356} is functioning as an uphill stepping stone, likely conformationally gated, in the long-range oxidation of C_{439}. This information starts to set the boundaries for the differences in redox potential between Y_{122} and Y_{356}. Unfortunately, spectrophotochemical methods to measure the redox potential of Y_{122} have been unsuccessful. Although an estimated value of 1000 ± 100 mV has been reported,[44] this number seems unlikely, as it is 100−200 mV higher than the redox potentials of Y in peptides reported in aqueous solution.[45−48] Some recent studies from our laboratory using $2,3,5\text{-}F_3Y^{\bullet}$ in place of Y_{122} to study nucleotide reduction suggest that this and other F_nY residues at positions 122 and 356 will soon allow us to bracket their differences in redox potential and the importance of conformational gating between these two Y residues in β2.[19]

In all the schemes describing PCET in RNR, W_{48} has a prominent role (Figure 1).[3,6] However, while it has long been established that this residue plays an essential role in electron transfer required to assemble the diferric $Y^{\bullet}$ cofactor in β2,[49,50] there is currently little support[51] for its involvement in the long-range radical propagation, and hence, we have left this residue in brackets in Figure 11. Finally, in Figure 11, we now have placed C_{439} at the same redox potential as Y_{730}, distinct from our previous models, on the basis of recent measurements made by Madej and Wardman.[52] If the redox potential difference between Y_{122}-β2 and C_{439}-α2 is several hundred millivolts, assuming an equilibrium of the radicals within the pathway, the amount of $C_{439}^{\bullet}$ would be ∼0.05% of $Y_{122}^{\bullet}$ at 25 °C. Given the expected rates for 2′-OH elimination of 10^6 to 10^9 s^{-1},[53−55] deoxynucleotide formation could still occur sufficiently fast to account for the rate of conformationally gated deoxynucleotide formation observed for wt-RNR (2−10 s^{-1}). Thus, the overall nucleotide reduction process would be pulled to the right by rapid, irreversible cleavage of the C2′−OH bond.[56]

The first observation of pathway tyrosyl radicals has also provided mechanistically important information on the structure and environment of Y residues located at the subunit interface in the active α2β2 complex. Unfortunately, atomic resolution information about the location of Y_{356} relative to β2 and to Y_{731} in α2 is still unavailable. EPR studies at 9 and 140 GHz and a recent crystal structure of NH_2Y_{731}-α2 provide additional insight into oxidation of Y residues at the subunit interface.

The **g** tensor of $Y^{\bullet}$ is only resolved by HF-EPR measurements, and it has been shown that the g_{xx} values are sensitive to electrostatic interactions of the protein environment and more specifically to H-bonding interactions.[36,57,58] The g_{xx} value for the $Y_{122}^{\bullet}$ equivalent from RNRs of different organisms ranges from 2.0092 in *E. coli*[36] to 2.0076 in mouse.[38] High-field electron−nuclear double resonance (ENDOR) spectroscopy has established that the mouse $Y^{\bullet}$ [58] and *Saccharomyces cerevisiae* $Y^{\bullet}$ [59] are H-bonded. While analysis of $Y_{356}^{\bullet}$ generated by $NO_2Y_{122}^{\bullet}$-β2 requires further studies by ENDOR spectroscopy to better simulate the spectra (Figure 6), the g_{xx} values of 2.0063 and 2.0073 for $Y_{356}^{\bullet}$ observed with wt-α2 and Y_{731}F-α2, respectively, are smaller than any previously reported g_{xx} values for $Y^{\bullet}$ radicals[35] and are likely indicative of their H-bonding/electrostatic environment. The differences between the wt and F mutant, in which a putative H-bonding partner has been removed, are intriguing and require further study.

The hfc associated with one of the β-^{1}H atoms of the $Y^{\bullet}$ radicals provides insight into Y's conformation within the active α2β2 complex and can be compared with structural data of Y itself to learn about their mobility. For example, the $Y_{122}^{\bullet}$ radicals in organisms that contain class Ia RNRs all have similar side chain orientations (A_{iso} = 55 MHz),[60] while $Y^{\bullet}$ radicals in the class Ib RNRs have similar, but distinct orientations compared to those in the Ia enzymes (Table S1, Supporting Information). Our tentative analysis of the hfc of $3,5\text{-}F_2Y_{731}$ gave a coupling of ∼40 MHz, indicating a distinct conformation relative to that observed in wt-α2 crystal structures. This conformation would prohibit colinear PCET between Y_{731} and Y_{730} in α2. We have recently reported a structure of NH_2Y_{730}-α2, where Y_{731} in one of three subunits in the asymmetric unit moved >9 Å from the conformation in the other subunits (Figure 8). Determination of θ from published crystallographic data for Y_{730} and Y_{731} reveals little variability in the case of residue 730 and much greater variability in the case of residue 731 (Table S1). Thus, being able to measure the hfc at position 731 in an RNR complex is required for thinking about the mechanism of PCET at the subunit interface.

Summary. Our observations demonstrate that $Y^{\bullet}$ radicals trapped in the pathway reside predominantly at Y_{356} in β2, with partial delocalization onto $Y_{731/730}$ in α2. This equilibrium distribution demonstrates an uphill redox gradient toward C_{439} oxidation, preventing accumulation of radical intermediates during long-range radical propagation. Structural information from EPR spectra at 9 and 140 GHz with several RNR variants suggests that the parallel orientation of Y_{731}-α2 and Y_{730}-α2 reported in the original X-ray structure of α2 may be different in

the active $\alpha2\beta2$ complex. These studies with combinations of unnatural amino acids site-specifically incorporated into each subunit of RNR are allowing us to understand in greater depth nature's design principles for this unprecedented long-range oxidation.

■ ASSOCIATED CONTENT

Supporting Information. LC−MS analysis of peptides from tryptic digestion of wt-$\alpha2$ and [β-$^2H_2$]Y-$\alpha2$, effects of sample preparation conditions on the PELDOR spectra, CW-EPR spectra of the reactions with [$NO_2Y_{122}^{\bullet}$]-$\beta2$/wt-$\alpha2$/ATP/CDP, time course of $NO_2Y^{\bullet}$ reduction and pathway radical formation, definition of θ, quantitation of [β-$^2H_2$]$Y^{\bullet}$ at 12, 24, and 60 ms and 25 °C, EPR spectral simulation of [β-$^2H_2$]$Y^{\bullet}$, Arrhenius plot of $NO_2Y^{\bullet}$ reduction in the [$NO_2Y_{122}^{\bullet}$]-$\beta2$/wt-$\alpha2$/ATP/CDP reaction, and summary of dihedral angles (θ) for the Y residues in $\alpha2$. This material is available free of charge via the Internet at http://pubs.acs.org.

■ AUTHOR INFORMATION

Corresponding Author
stubbe@mit.edu

■ ACKNOWLEDGMENT

This work was supported by NIH Grants GM29595 (to J.S.) and EB002804 and EB002026 (to R.G.G.). B.C. was supported by a DFG research fellowship (Grant CO802/1-1). We thank Dr. Ralph T. Weber for assistance in the PELDOR measurements.

■ REFERENCES

(1) Stubbe, J.; van der Donk, W. A. *Chem. Rev.* **1998**, *98*, 705–762.
(2) Nordlund, P.; Reichard, P. *Annu. Rev. Biochem.* **2006**, *75*, 681–706.
(3) Uhlin, U.; Eklund, H. *Nature* **1994**, *370*, 533–539.
(4) Stubbe, J.; Nocera, D.; Yee, C. S.; Chang, M. C. Y. *Chem. Rev.* **2003**, *103*, 2167–2201.
(5) Yokoyama, K.; Uhlin, U.; Stubbe, J. *J. Am. Chem. Soc.* **2010**, *132*, 15368–15379.
(6) Reece, S. Y.; Hodgkiss, J. M.; Stubbe, J.; Nocera, D. G. *Philos. Trans. R. Soc., B* **2006**, *361*, 1351–1364.
(7) Ge, J.; Yu, G.; Ator, M. A.; Stubbe, J. *Biochemistry* **2003**, *42*, 10071–10083.
(8) Ekberg, M.; Sahlin, M.; Eriksson, M.; Sjöberg, B.-M. *J. Biol. Chem.* **1996**, *271*, 20655–20659.
(9) Climent, I.; Sjöberg, B.-M.; Huang, C. Y. *Biochemistry* **1992**, *31*, 4801–4807.
(10) Seyedsayamdost, M. R.; Stubbe, J. *J. Am. Chem. Soc.* **2006**, *128*, 2522–2523.
(11) Seyedsayamdost, M. R.; Xie, J.; Chan, C. T.; Schultz, P. G.; Stubbe, J. *J. Am. Chem. Soc.* **2007**, *129*, 15060–15071.
(12) Bennati, M.; Robblee, J. H.; Mugnaini, V.; Stubbe, J.; Freed, J. H.; Borbat, P. *J. Am. Chem. Soc.* **2005**, *127*, 15014–15015.
(13) Wang, J.; Lohman, G. J.; Stubbe, J. *Proc. Natl. Acad. Sci. U.S.A.* **2007**, *104*, 14324–14329.
(14) Schiemann, O.; Prisner, T. F. *Q. Rev. Biophys.* **2007**, *40*, 1–53.
(15) Seyedsayamdost, M. R.; Chan, C. T.; Mugnaini, V.; Stubbe, J.; Bennati, M. *J. Am. Chem. Soc.* **2007**, *129*, 15748–15749.
(16) Bennati, M.; Weber, A.; Antonic, J.; Perlstein, D. L.; Robblee, J.; Stubbe, J. *J. Am. Chem. Soc.* **2003**, *125*, 14988–14989.
(17) Seyedsayamdost, M. R.; Reece, S. Y.; Nocera, D. G.; Stubbe, J. *J. Am. Chem. Soc.* **2006**, *128*, 1569–1579.
(18) Salowe, S. P.; Ator, M. A.; Stubbe, J. *Biochemistry* **1987**, *26*, 3408–3416.
(19) Minnihan, E. C.; Young, D.; Schultz, P. G.; Stubbe, J. *J. Am. Chem. Soc.* 2011, *133*, 15942–15945.
(20) Yokoyama, K.; Uhlin, U.; Stubbe, J. *J. Am. Chem. Soc.* **2010**, *132*, 8385–8397.
(21) Thelander, L. *J. Biol. Chem.* **1973**, *248*, 4591–4601.
(22) Atkin, C. L.; Thelander, L.; Reichard, P.; Lang, G. *J. Biol. Chem.* **1973**, *248*, 7464–7472.
(23) Pannier, M.; Veit, S.; Godt, A.; Jeschke, G.; Spiess, H. W. *J. Magn. Reson.* **2000**, *142*, 331–340.
(24) Jeschke, G.; Chechik, V.; Ionita, P.; Godt, A.; Zimmermann, H.; Banham, J.; Timmel, C. R.; Hilger, D.; Jung, H. *Appl. Magn. Reson.* **2006**, *30*, 473–498.
(25) Chiang, Y. W.; Borbat, P. P.; Freed, J. H. *J. Magn. Reson.* **2005**, *172*, 279–295.
(26) Becerra, L. R.; Gerfen, G. J.; Bellew, B. F.; Bryant, J. A.; Hall, D. A.; Inati, S. J.; Weber, R. T.; Un, S.; Prisner, T. F.; McDermott, A. E.; Fishbein, K. W.; Kreischer, K. E.; Temkin, R. J.; Singel, D. J.; Griffin, R. G. *J. Magn. Reson.* **1995**, *117*, 28–40.
(27) Bennati, M.; Farrar, C. T.; Bryant, J. A.; Inati, S. J.; Weis, V.; Gerfen, G. J.; Riggs-Gelasco, P.; Stubbe, J.; Griffin, R. G. *J. Magn. Reson.* **1999**, *138*, 232–243.
(28) Hahn, E. L. *Phys. Rev.* **1950**, *80*, 580–594.
(29) Palmer, G. *Methods Enzymol.* **1967**, *10*, 595.
(30) Stoll, S.; Schweiger, A. *J. Magn. Reson.* **2006**, *178*, 42–55.
(31) Baudot, A.; Alger, L.; Boutron, P. *Cryobiology* **2000**, *40*, 151–158.
(32) Biglino, D.; Schmidt, P. P.; Reijerse, E. J.; Lubitz, W. *Phys. Chem. Chem. Phys.* **2006**, *8*, 58–62.
(33) The relative ratio of the 30 and 33 Å peaks changed upon introduction of the Y731F mutation (compare parts D and H of Figure 5). The significance of this observation is currently unknown as multiple factors, such as the fitting quality and the relaxation properties of the radicals, could affect the ratio of the peaks.
(34) Seyedsayamdost, M. R.; Argirević, T.; Minnihan, E. C.; Stubbe, J.; Bennati, M. *J. Am. Chem. Soc.* **2009**, *131*, 15729–15738.
(35) Svistunenko, D. A.; Cooper, C. E. *Biophys. J.* **2004**, *87*, 582–595.
(36) Gerfen, G. J.; Bellew, B. F.; Un, S.; Bollinger, J. M.; Stubbe, J.; Griffin, R. G.; Singe, D. J. *J. Am. Chem. Soc.* **1993**, *115*, 6420–6421.
(37) Tommos, C.; Tang, X.-S.; Wamcke, K.; Hoganson, C. W.; Styring, S.; McCracken, J.; Diner, B. A.; Babcock, G. T. *J. Am. Chem. Soc.* **1995**, *117*, 10325–10335.
(38) Schmidt, P. P.; Andersson, K. K.; Barra, A. L.; Thelander, L.; Gräslund, A. *J. Biol. Chem.* **1996**, *271*, 23615–23618.
(39) Unfortunately, the signals associated with $F2Y^{\bullet}$ are not sufficiently intense to allow successful PELDOR experiments.
(40) Fessenden, R. W.; Schuler, R. H. *J. Chem. Phys.* **1963**, *39*, 2147–2195.
(41) Eriksson, M.; Uhlin, U.; Ramaswamy, S.; Ekberg, M.; Regnstrom, K.; Sjöberg, B.-M.; Eklund, H. *Structure* **1997**, *5*, 1077–1092.
(42) Minnihan, E. C.; Seyedsayamdost, M. R.; Uhlin, U.; Stubbe, J. *J. Am. Chem. Soc.* **2011**, *133*, 9430–9440.
(43) Seyedsayamdost, M. R.; Yee, C. S.; Reece, S. Y.; Nocera, D. G.; Stubbe, J. *J. Am. Chem. Soc.* **2006**, *128*, 1562–1568.
(44) Silva, K. E.; Elgren, T. E.; Que, L., Jr.; Stankovich, M. T. *Biochemistry* **1995**, *34*, 14093–14103.
(45) Yee, C. S.; Seyedsayamdost, M. R.; Chang, M. C.; Nocera, D. G.; Stubbe, J. *Biochemistry* **2003**, *42*, 14541–14552.
(46) Tommos, C.; Skalicky, J. J.; Pilloud, D. L.; Wand, A. J.; Dutton, P. L. *Biochemistry* **1999**, *38*, 9495–9507.
(47) DeFelippis, M. R.; Murthy, C. P.; Broitman, F.; Weinraub, D.; Faraggi, M.; Klapper, M. H. *J. Phys. Chem.* **1991**, *95*, 3416–3419.
(48) We have been using 0.83 V for the E_p of Y at pH 7.0 on the basis of ref 46 and our independent measurement. Pulse radiolysis methods, however, report a value of 0.93 V, as in ref 47 and references therein.
(49) Baldwin, J.; Krebs, C.; Ley, B. A.; Edmondson, D. E.; Huynh, B. H.; Bollinger, J. M. *J. Am. Chem. Soc.* **2000**, *122*, 12195–12206.

(50) Bollinger, J. M.; Tong, W. H.; Ravi, N.; Huynh, B. H.; Edmonson, D. E.; Stubbe, J. *J. Am. Chem. Soc.* **1994**, *116*, 8024–8032.
(51) Rova, U.; Goodtzova, K.; Ingemarson, R.; Behravan, G.; Gräslund, A.; Thelander, L. *Biochemistry* **1995**, *34*, 4267–4275.
(52) Madej, E.; Wardman, P. *Arch. Biochem. Biophys.* **2007**, *462*, 94–102.
(53) Steenken, S.; Davies, M. J.; Gilbert, B. C. *J. Chem. Soc., Perkin Trans. 2* **1986**, 1003–1010.
(54) Bansal, K. M.; Grätzel, M.; Henglein, A.; Janata, E. *J. Phys. Chem.* **1973**, *77*, 16–19.
(55) Lenz, R.; Giese, B. *J. Am. Chem. Soc.* **1997**, *119*, 2784–2794.
(56) Licht, S.; Stubbe, J. *Compr. Nat. Prod. Chem.* **1999**, *5*, 163–203.
(57) Hoganson, C. W.; Babcock, G. T. *Biochemistry* **1992**, *31*, 11874–11880.
(58) van Dam, P. J.; Willems, J.-P.; Schmidt, P. P.; Pötsch, P.; Barra, A. L.; Hagen, W. R.; Hoffman, B. M.; Andersson, K. K.; Gräslund, A. *J. Am. Chem. Soc.* **1998**, *120*, 5080–5085.
(59) Bar, G.; Bennati, M.; Nguyen, H. H.; Ge, J.; Stubbe, J. A.; Griffin, R. G. *J. Am. Chem. Soc.* **2001**, *123*, 3569–3576.
(60) Lendzian, F. *Biochim. Biophys. Acta* **2005**, *1707*, 67–90.
(61) Högbom, M.; Andersson, M. E.; Nordlund, P. *J. Biol. Inorg. Chem.* **2001**, *6*, 315–323.